REPORT DOCUMENTATION PAGE

Form Approved OMB NO. 0704-0188

1. REPORT DATE (DD-MM-YYYY)	2. REPORT TYPE	3. DATES COVERED (From - To)
27-08-2013	Final Report	15-Apr-2009 - 14-Apr-2013

4. TITLE AND SUBTITLE
Spatial Brain Control Interface using Optical and Electrophysiological Measures

5a. CONTRACT NUMBER
W911NF-09-1-0116

5b. GRANT NUMBER

5c. PROGRAM ELEMENT NUMBER
611102

6. AUTHORS
Barbara Heider

5d. PROJECT NUMBER

5e. TASK NUMBER

5f. WORK UNIT NUMBER

7. PERFORMING ORGANIZATION NAMES AND ADDRESSES
Rutgers, The State University of New Jersey - Ne
180 University Ave
Newark, NJ 07102 -1803

8. PERFORMING ORGANIZATION REPORT NUMBER

9. SPONSORING/MONITORING AGENCY NAME(S) AND ADDRESS(ES)
U.S. Army Research Office
P.O. Box 12211
Research Triangle Park, NC 27709-2211

10. SPONSOR/MONITOR'S ACRONYM(S)
ARO

11. SPONSOR/MONITOR'S REPORT NUMBER(S)
55897-LS.3

12. DISTRIBUTION AVAILIBILITY STATEMENT
Approved for Public Release; Distribution Unlimited

13. SUPPLEMENTARY NOTES
The views, opinions and/or findings contained in this report are those of the author(s) and should not contrued as an official Department of the Army position, policy or decision, unless so designated by other documentation.

14. ABSTRACT
Functional imaging and electrical recordings were performed over posterior parietal cortex during a spatial attention task. Subjects had to covertly shift their attention with simultaneous visual stimulation and motor planning. The imaging response showed modulation for spatial conditions. Various analysis and decoding methods were assessed to extract a prediction signature from this brain activity. The Linear Support Vector Machine (LSVM) was the most appropriate for implementing a reliable brain-computer interface (BCI). The LSVM method

15. SUBJECT TERMS
brain imaging, electrical neuron activity, statistical analysis, brain-computer interface

16. SECURITY CLASSIFICATION OF:			17. LIMITATION OF ABSTRACT	15. NUMBER OF PAGES	19a. NAME OF RESPONSIBLE PERSON
a. REPORT	b. ABSTRACT	c. THIS PAGE			Barbara Heider
UU	UU	UU	UU		19b. TELEPHONE NUMBER: 973-353-3249

Report Title

Spatial Brain Control Interface using Optical and Electrophysiological Measures

ABSTRACT

Functional imaging and electrical recordings were performed over posterior parietal cortex during a spatial attention task. Subjects had to covertly shift their attention with simultaneous visual stimulation and motor planning. The imaging response showed modulation for spatial conditions. Various analysis and decoding methods were assessed to extract a prediction signature from this brain activity. The Linear Support Vector Machine (LSVM) was the most appropriate for implementing a reliable brain-computer interface (BCI). The LSVM method was applied to the imaging data with various temporal parameters. All variations proved to be suitable to predict experimental parameters (left vs. right eye movement) from the hemodynamic response over PPC. However, due to the slow hemodynamic signal, performance for the LSVM reached only ~60% during the later task phases. Thus, the subject's response could not be predicted reliably before the actual movement. Electrophysiological recordings (single unit and local field potentials) were performed in the previously imaged regions to allow comparison with the hemodynamic response. These electrical signals especially the local field potentials proved to be fast and strongly tuned for the spatial parameters of the task. Thus, a reliable BCI that can predict upcoming movements or behaviors will need to combine signals from various sources.

Enter List of papers submitted or published that acknowledge ARO support from the start of the project to the date of this printing. List the papers, including journal references, in the following categories:

(a) Papers published in peer-reviewed journals (N/A for none)

Received		Paper
08/21/2013	2.00	Barbara Heider, Ralph M. Siegel. Optical imaging of visually guided reaching in macaque posterior parietal cortex, Brain Structure and Function, (02 2013): 0. doi:
TOTAL:	**1**	

Number of Papers published in peer-reviewed journals:

(b) Papers published in non-peer-reviewed journals (N/A for none)

Received		Paper
TOTAL:		

Number of Papers published in non peer-reviewed journals:

(c) Presentations

Muñoz Silva F, Heider B, Siegel RM (2012) Task-related modulation of local field potential spectral content in macaque parietal cortex during a spatial attention task. In: Society for Neuroscience, Program No. 673.01. New Orleans, LA: 2012 Abstract Viewer/Itinerary Planner.

Number of Presentations: 1.00

Non Peer-Reviewed Conference Proceeding publications (other than abstracts):

Received	Paper

TOTAL:

Number of Non Peer-Reviewed Conference Proceeding publications (other than abstracts):

Peer-Reviewed Conference Proceeding publications (other than abstracts):

Received	Paper

TOTAL:

Number of Peer-Reviewed Conference Proceeding publications (other than abstracts):

(d) Manuscripts

Received		Paper
04/24/2012	1.00	Barbara Heider, Ralph M. Siegel. Optical Imaging During Visually Guided Reaching in Macaque Posterior Parietal Cortex, NeuroImage (04 2012)

TOTAL: **1**

Number of Manuscripts:

Books

Received	Paper

TOTAL:

Patents Submitted

Patents Awarded

Awards

Graduate Students

NAME	PERCENT_SUPPORTED
FTE Equivalent:	
Total Number:	

Names of Post Doctorates

NAME	PERCENT_SUPPORTED
Fabian Munoz Silva	0.90
FTE Equivalent:	**0.90**
Total Number:	**1**

Names of Faculty Supported

NAME	PERCENT_SUPPORTED	National Academy Member
Barbara Heider	0.56	No
FTE Equivalent:	**0.56**	
Total Number:	**1**	

Names of Under Graduate students supported

NAME	PERCENT_SUPPORTED
FTE Equivalent:	
Total Number:	

Student Metrics

This section only applies to graduating undergraduates supported by this agreement in this reporting period

The number of undergraduates funded by this agreement who graduated during this period:	0.00
The number of undergraduates funded by this agreement who graduated during this period with a degree in science, mathematics, engineering, or technology fields:.....	0.00
The number of undergraduates funded by your agreement who graduated during this period and will continue to pursue a graduate or Ph.D. degree in science, mathematics, engineering, or technology fields:.....	0.00
Number of graduating undergraduates who achieved a 3.5 GPA to 4.0 (4.0 max scale):	0.00
Number of graduating undergraduates funded by a DoD funded Center of Excellence grant for Education, Research and Engineering:	0.00
The number of undergraduates funded by your agreement who graduated during this period and intend to work for the Department of Defense	0.00
The number of undergraduates funded by your agreement who graduated during this period and will receive scholarships or fellowships for further studies in science, mathematics, engineering or technology fields:	0.00

Names of Personnel receiving masters degrees

NAME
Total Number:

Names of personnel receiving PHDs

NAME
Total Number:

Names of other research staff

NAME	PERCENT_SUPPORTED
Jasmine Siegel	0.50
FTE Equivalent:	**0.50**
Total Number:	**1**

Sub Contractors (DD882)

Inventions (DD882)

Scientific Progress

See Attachments

Technology Transfer

Final Report for Award W911NF-09-1-0116 (ending 4/15/2013)

(1) Rationale

The first step of the project was to perform intrinsic optical imaging and electrophysiological recordings in posterior parietal cortex (PPC) of non-human primates (NHP). Two areas on the surface of the cortex were selected: area 7a and the dorsal prelunate (DP) while the NHP performed a visual spatial attention task. Previous studies from this laboratory demonstrate that PPC is strongly modulated by eye position and plays a crucial role in attentional processing (Raffi & Siegel, 2005; Quraishi *et al.*, 2007) and motor planning for visually guided eye and hand movements (Heider & Siegel, 2013). The intrinsic signal is characterized by relatively high spatial resolution in the range of ~100 µm compared to other hemodynamic imaging techniques such as functional magnetic resonance imaging (fMRI). Electrophysiological recordings on the other hand have high temporal precision (<0.1 ms). Various analyses were performed on the optical imaging and electrophysiological data to extract information from the two PPC areas most likely related to the NHP's behavior. Of particular interest was the prediction of the locus of attention, which corresponds to the saccade target.

Thus, the second step of the project was the classification of the experimental conditions (locus of attention, eye position) based on the imaging and electrophysiological recordings. The main goal is to predict the experimental conditions from the cortical activity in PPC. Generating a reliable decoder will form the basis to create a brain-computer interface (BCI) that can predict the upcoming behaviors of the subject before the motor plan is executed. In order to optimize the decoding of the brain signals, multiple analysis approaches have been evaluated and tested over large numbers of experiments and conditions.

(2) Task and Experimental Design

The NHP performed a visual spatial attention task (Fig. 1) based on previous publications (Raffi & Siegel, 2005). A trial starts with the onset of a central fixation dot, which prompts the NHP to start fixation within 500 ms. After one second, a small cue stimulus (0.3º gray diamond) on either the left or right side of the fixation dot was displayed for 400 ms. Two seconds after trial start, two identical stimuli (white squares 10° visual angle) were presented at 10º eccentricity on either side of the fixation dot. The NHP had to maintain central fixation but was instructed by the cue to which stimulus of the pair attention had to be directed. After a variable time interval (2000-2500 ms), the cued stimulus dimmed slightly and the NHP had to saccade to the changed stimulus within a 500 ms reaction time window. Successful completion of a trial was rewarded with a drop of juice. An incorrect trial was aborted immediately and no reward was given. Optical and electrophysiological recordings were performed during the entire trial period of approximately 6.5 s.

This basic task was performed in two versions to control for the effects of instructed locus of attention. 1) Cued condition, as described above (Fig. 1A). 2) Non-cued condition, that is, the NHP was not being instructed which side of the display was going to change (Fig. 1B). In the latter condition, attention could not be directed to a particular stimulus location but rather was divided or switching back and forth between the two locations. The use of these two conditions was specifically designed to enable the

separation of the attentional or planning from the motor aspect of the eye movement. The basic task was performed in the primary position (i.e., fixation point is straight ahead) or the entire test coordinate system can be shifted up or down in order to contrast gain fields with locus of spatial attention. Typically, one imaging run consisted of about 400 trials (duration ~1.5 hours). On many imaging sessions (days) data from 2 runs could be collected.

(3) Data Collection

Intrinsic optical imaging data were collected from the left hemisphere of one NHP (M3L). More than 50 experiments were performed in this first series. Additional optical imaging data from the right hemisphere of another NHP (M1R) were added to allow comparison between subjects and experimental parameters. In M3L, additional electrophysiological recordings were performed over the cortical regions that had been imaged previously. Thus, electrophysiological and optical (hemodynamic) signals can be compared directly over the same cortical regions during different stages of the task to optimize performance of the BCI (Zimmermann *et al.*, 2011; Fazli *et al.*, 2012).

Imaging: Intrinsic optical imaging allows measuring changes in blood oxygenation during a given task using reflectance of the cortical tissue. The exposed cortex is covered by a transparent artificial dura and illuminated with orange light (625 nm). Under these conditions, the amount of reflected light is proportional to the proportion of oxygenated and deoxygenated hemoglobin in the tissue and thus can be considered an indirect indicator of cortical activity. We decided against utilizing voltage sensitive dye (VSD) imaging over the same cortical areas. The potential advantage of this form of imaging is the fast and direct neural signal. However, for imaging in behaving NHP, this method has serious drawbacks and thus proved to be unsuitable. One problem was the fact that the cortex has be infused repeatedly with the non-toxic dye for several hours prior to imaging while the NHP is required to wait in the primate chair (Slovin *et al.*, 2002). This prolonged waiting period (2-3 hours) compromised the cooperation of the NHP in the subsequent imaging experiments. In addition, the staining of the cortex made it difficult to illuminate the cortex sufficiently.

Electrophysiology: Targeted recordings were performed either through the artificial dura or through the regrown native dura after removal of the artificial dura. Basic methods and related data have been described previously (Heider *et al.*, 2010). Single-unit and multi-unit activity (SUA and MUA) are the spiking activity from one or several recorded neurons. This activity represents the output of neurons. At the same time, local field potentials (LFP) can be measured, which represent average synaptic input activity from thousands of neurons. These electrical signals were recorded extracellularly from fine, glass-insulated Pt-Ir electrodes in targeted cortical locations. As expected, spiking activity and LFP generally did not match with respect to their spatial tuning (see Figs. 15 and 17 of Attachment). Previous imaging studies further suggest that LFPs correlate more strongly with the hemodynamic response (Logothetis *et al.*, 2001). Activity from a total of 54 neurons was recorded from areas 7a and DP from M3L. The electrical signal was analyzed offline and spiking activity and LFPs were synchronized with the stimulus onset (*pre*) and saccade events (*post*), and the resulting values compared between conditions.

(4) Basic Imaging Results

The reflectance signal followed the typical biphasic time course over the course of the trial (Figs. 2A, 5A), that is, an increase in reflectance with a peak at ~2 s after stimulus onset (overshoot) and a subsequent decrease (undershoot). This temporal profile of the hemodynamic response was similar in both areas. Therefore, it is important to remember that the hemodynamic response lags behind the crucial event by about 1.5 s. Linear regression coefficients were extracted pixel-by-pixel from the reflectance signal by fitting the spatial parameters (eye position, vertical a_y; locus of attention, horizontal a_x) and mean reflectance (intercept a_0), as published previously (Siegel *et al.*, 2003; Raffi & Siegel, 2005). Over the course of the trial the values of the various regression parameters increased and peaked at 1.5-2 s after stimulus onset (Figs. 2B, 5B). These regression parameters and their corresponding time course varied considerably between experiments (Figs. 3, 4). This variability was also observed for the non-cued experiments (Figs. 6, 7). The time course of the reflectance signal was not substantially different during the non-cued task condition (compare Fig. 5 with Fig. 2). These combined results confirm that the intrinsic reflectance signal displayed a typical temporal profile over the course of a trial. Despite this consistency, the selectivity of the reflectance signal for the experimental parameters varied considerably between experiments (Figs. 3, 4, 6,7).

(5) Data Analysis and Decoding

Two main challenges were encountered when utilizing intrinsic optical imaging as a basis for a BCI: First, the intrinsic signal is inherently slow so that it takes at least 1.5 s after stimulus onset to generate reliable maps (Figs. 2B, 5B). Signal separation between experimental conditions peaked even later (2-3 s). However, for prediction, it is important to extract a useful signature as early as possible. Second, the intra-subject variability across experiments (Figs. 3, 4, 6, 7) made it difficult to establish a decoding mechanism that would operate reliably across days. Thus, a wide selection of prediction and decoding routines has to be evaluated so that a useful signal can be extracted from the noisy and variable data.

The main goal was the extract parameters from the reflectance images of the cortex that allow prediction of the experimental parameters that guide the behavior of the NHP. By selecting the most accurate and reliable classification algorithm, we can attempt to build a BCI capable of predicting the NPH's upcoming behavior based on the hemodynamic activity in PPC. It is important to consider that we can only evaluate one hemisphere at a time. This differs from approaches using whole brain imaging such a multi-channel near infra-red spectroscopy (NIRS) (Herrmann *et al.*, 2005).

Support Vector Machine (SVM) is based on a statistical learning approach that allows mapping of experimental or behavioral conditions onto the cortex. SVM does not imply assumptions about the distribution of the signal or the noise. Various SVM classifiers were applied to the imaging data. Linear kernels (LSVM) allow direct mapping of the classification performance onto the cortical map (LaConte *et al.*, 2005; Xiao *et al.*, 2008), as illustrated in Figs 9,10,12,13. As the prediction of attentional locus was the main goal of the current project, upper and lower eye positions were analyzed separately to allow a binary classification. First, a training set was assembled from randomly selected trials (10% of the original data set). The remainder of the data was

used to test the decoder (cross validation). The goal of the training was to find the hyperplane (Fig. 8A) that could distinguish between the two classes (left *vs*. right locus of attention). The optimal hyperplane is the one with a maximal margin of separation between the two classes (Fig. 8B). This hyperplane serves as a decision function that can be used for classifying a test example. Depending on the learning method there are many possible solutions or hyperplanes. The temporal profile of the reflectance signal demonstrated that the separation between classes increased over time (Figs. 2-6), thus two methods were chosen for the assembly of the data with respect to training set.

First, all 47 frames were included to calculate the weight vector for classification (Figs. 9,10), which was then applied to the test data separately for different time segments (always 4 frames averaged). Thus, the entire time course was included in the training set and thus contained frames early in the trial that did not contain any relevant signals. For the illustrated sample experiments, the resulting average prediction accuracy across all time segments ranged from 60-66% for the cued task, and from 53-61% for the non-cued task. The prediction strength was distributed in a patchy manner across the cortex and also varied strongly between time segments. The difference in accuracy between cued and non-cued condition were not significant (Fig. 11) but overall accuracy using this method was significantly greater than chance level (50%).

Second, the training and testing was performed separately for each time segment (4 frames) to assess the temporal profile of the prediction accuracy (Figs. 12,13). Thus, the vector for the training set contained only 4 frames. Prediction accuracy increased over time and reached a maximum around 3 s after stimulus onset. Earlier time segments yielded accuracies around chance level. The color-coded projections of the test classification onto the cortex again showed a patchy topographical distribution of the predicted experimental parameters (locus of attention). However, there was little consistency between experiments as demonstrated when plotting accuracy over time separately for each experiment and condition (Fig. 14).

Thus, based on the results from both methods it is clear that neither approach yielded satisfactory prediction accuracies, which is mostly due to the slow hemodynamic response and the variability of the responses over PPC (Raffi & Siegel, 2005; Raffi & Siegel, 2007). A decoder would need to be recalibrated from one experiment to the next, which is impractical for the current project.

Electrophysiological recordings provide much greater temporal resolution than the hemodynamic signal, that is, spiking and LFP responses happen almost instantaneously. One example neuron from each area illustrates the variety of spike modulation with the spatial (eye position, attentional locus) and temporal (event synchronization) task parameters (Fig. 15). The area 7a neuron had sparse firing and was weakly modulated by the spatial parameters during either task. However, the non-cued task yielded overall higher firing rate. The area DP neuron had higher firing rates and was strongly modulated by the spatial parameters and the saccade response. These differences were confirmed in the population of neurons by plotting the average firing rate for the 1 s epoch after stimulus onset against to the average firing rate for the epoch after saccade onset separately for each neuron (Fig. 16).

LFP recordings from the same site as the single neuron examples showed different modulations than the single spike results (Fig. 17). Strong increases in power across many frequencies (10-80 Hz) were observed for the 7a site (same as for single neuron

in Fig. 15) before stimulus onset indicative of a strong anticipatory modulation, which was present during cued and non-cued conditions. Such increases in power were absent in the DP site. The average spectrogram was calculated for each epoch and recording site and plotted separately for each area (Fig. 18). Consistently, area 7a sites were more strongly modulated than the DP sites in particular for the cued attention task. This suggests that LFP data could provide essential information regarding separation temporal and spatial task parameters, which has been confirmed in another PPC area, the so-called *parietal reach region* PRR (Scherberger *et al.*, 2005). The inter-areal differences with respect to spiking *vs.* LFP measurements suggest that connections from DP to 7a are directed from single neuron to *node* (network).

(6) Conclusions

Based on the current imaging and electrophysiological findings it could be concluded that areas 7a and DP are not ideal cortical candidates for a BCI application. Other cortical areas such as motor or sensory cortices have proven to be suitable for BCI application both in human and non-human primates (O'Leary & Hatsopoulos, 2006; Truccolo *et al.*, 2008; Vargas-Irwin *et al.*, 2010). However, PPC might offer other advantages namely adaptability and flexibility, due to the representation of cognitive variables (Hauschild *et al.*, 2012). Unlike the lateral intraparietal (LIP) or PRR, which contain relatively stable representations for saccade target and reach targets (Snyder *et al.*, 2000; Scherberger *et al.*, 2003), areas 7a and DP do not have very precise spatial representations (Heider *et al.*, 2005; Raffi & Siegel, 2005). These two areas have variable representations that indicate a high degree of flexibility, which might be beneficial in changing environments. Our and other results suggest that the ideal BCI will consist of a combination of areas that combine stable and flexible representations. Moreover, brain activity from various sources should be utilized, hemodynamic (e.g., optical) for the spatial specificity and electrophysiological (e.g., EEG) for the temporal resolution.

(7) References

Fazli, S., Mehnert, J., Steinbrink, J., Curio, G., Villringer, A., Müller, K.-R. & Blankertz, B. (2012) Enhanced performance by a hybrid NIRS-EEG brain computer interface. *Neuroimage*, **59**, 519-529.

Hauschild, M., Mulliken, G.H., Fineman, I., Loeb, G.E. & Andersen, R.A. (2012) Cognitive signals for brain–machine interfaces in posterior parietal cortex include continuous 3D trajectory commands. *Proceedings of the National Academy of Sciences*, **109**, 17075-17080.

Heider, B., Jandó, G. & Siegel, R.M. (2005) Functional architecture of retinotopy in visual association cortex of behaving monkey. *Cereb. Cortex*, **15**, 460-478.

Heider, B., Karnik, A., Ramalingam, N. & Siegel, R.M. (2010) Neural Representation During Visually Guided Reaching in Macaque Posterior Parietal Cortex. *J. Neurophysiol.*, **104**, 3494-3509.

Heider, B. & Siegel, R.M. (2013) Optical imaging of visually guided reaching in macaque posterior parietal cortex. *Brain Structure and Function*, doi: 10.1007/s00429-00013-00513-y.

Herrmann, M.J., Ehlis, A.C., Wagener, A., Jacob, C.P. & Fallgatter, A.J. (2005) Near-infrared optical topography to assess activation of the parietal cortex during a visuo-spatial task. *Neuropsychologia*, **43**, 1713-1720.

LaConte, S., Strother, S., Cherkassky, V., Anderson, J. & Hu, X. (2005) Support vector machines for temporal classification of block design fMRI data. *Neuroimage*, **26**, 317-329.

Logothetis, N.K., Pauls, J., Augath, M., Trinath, T. & Oeltermann, A. (2001) Neurophysiological investigation of the basis of the fMRI signal. *Nature*, **412**, 150-157.

O'Leary, J.G. & Hatsopoulos, N.G. (2006) Early Visuomotor Representations Revealed From Evoked Local Field Potentials in Motor and Premotor Cortical Areas. *J. Neurophysiol.*, **96**, 1492-1506.

Quraishi, S., Heider, B. & Siegel, R.M. (2007) Attentional modulation of receptive field structure in area 7a of the behaving monkey. *Cereb. Cortex*, **17**, 1841-1857.

Raffi, M. & Siegel, R.M. (2005) Functional Architecture of Spatial Attention in the Parietal Cortex of the Behaving Monkey. *J. Neurosci.*, **25**, 5171-5186.

Raffi, M. & Siegel, R.M. (2007) A functional architecture of optic flow in the inferior parietal lobule of the behaving monkey. *PLoS One*, **2**, e200.

Scherberger, H., Goodale, M.A. & Andersen, R.A. (2003) Target selection for reaching and saccades share a similar behavioral reference frame in the macaque. *J. Neurophysiol.*, **89**, 1456-1466.

Scherberger, H., Jarvis, M.R. & Andersen, R.A. (2005) Cortical Local Field Potential Encodes Movement Intentions in the Posterior Parietal Cortex. *Neuron*, **46**, 347-354.

Siegel, R.M., Raffi, M., Phinney, R.E., Turner, J.A. & Jandó, G. (2003) Functional architecture of eye position gain fields in visual association cortex of behaving monkey. *J. Neurophysiol.*, **90**, 1279-1294.

Slovin, H., Arieli, A., Hildesheim, R. & Grinvald, A. (2002) Long-term voltage-sensitive dye imaging reveals cortical dynamics in behaving monkeys. *J. Neurophysiol.*, **88**, 3421-3438.

Snyder, L.H., Batista, A.P. & Andersen, R.A. (2000) Intention-related activity in the posterior parietal cortex: a review. *Vis. Res.*, **40**, 1433-1441.

Truccolo, W., Friehs, G.M., Donoghue, J.P. & Hochberg, L.R. (2008) Primary Motor Cortex Tuning to Intended Movement Kinematics in Humans with Tetraplegia. *J. Neurosci.*, **28**, 1163-1178.

Vargas-Irwin, C.E., Shakhnarovich, G., Yadollahpour, P., Mislow, J.M.K., Black, M.J. & Donoghue, J.P. (2010) Decoding Complete Reach and Grasp Actions from Local Primary Motor Cortex Populations. *J. Neurosci.*, **30**, 9659-9669.

Xiao, Y., Rao, R., Cecchi, G. & Kaplan, E. (2008) Improved mapping of information distribution across the cortical surface with the support vector machine. *Neural Netw.*, **21**, 341-348.

Zimmermann, R., Marchal-Crespo, L., Lambercy, O., Fluet, M.C., Riener, R., Wolf, M. & Gassert, R. (2011) Towards a BCI for sensorimotor training: Initial results from simultaneous fNIRS and biosignal recordings. Engineering in Medicine and Biology Society, EMBC, 2011 Annual International Conference of the IEEE. Boston, MA. p. 6339-6343.

Figure 1

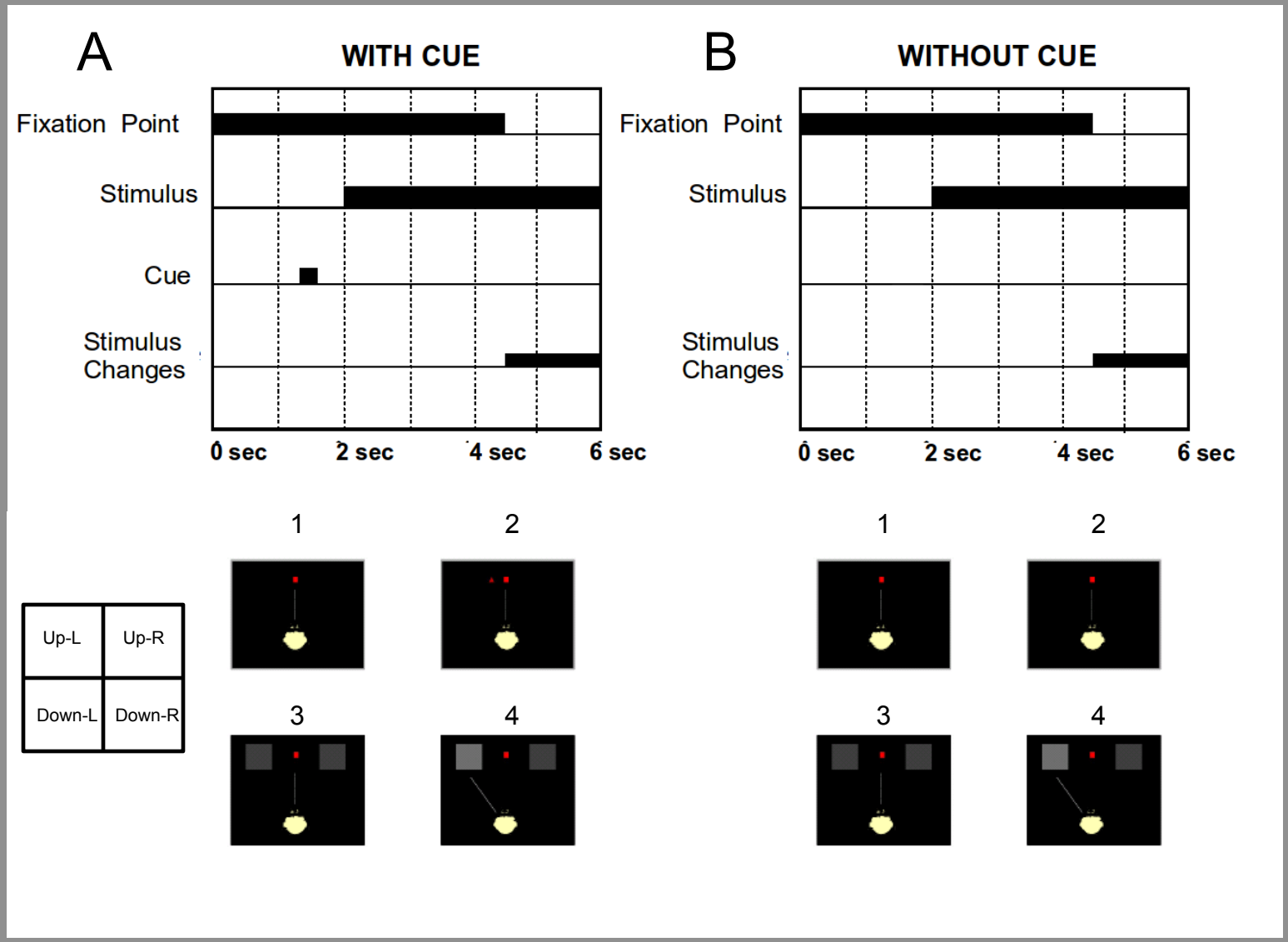

Task sequence (top) and task display (bottom) for cued (A) and non-cued (B) spatial attention task: 1) start fixation, 2) cue (to left), 3) stimulus pair (left and right targets), 4) stimulus change (left) and start saccade.

Figure 2

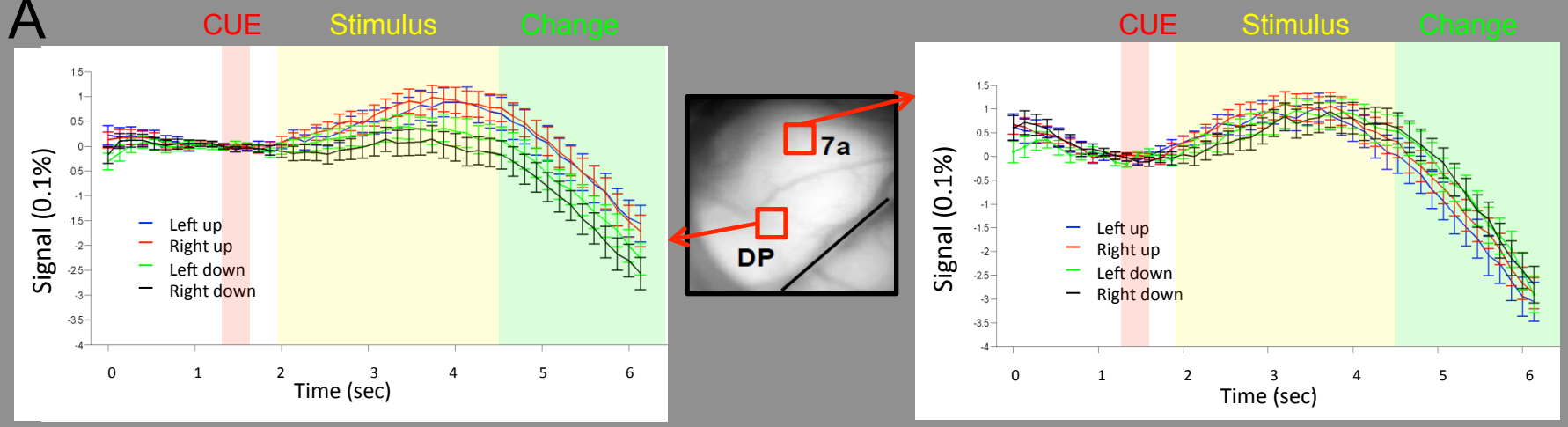

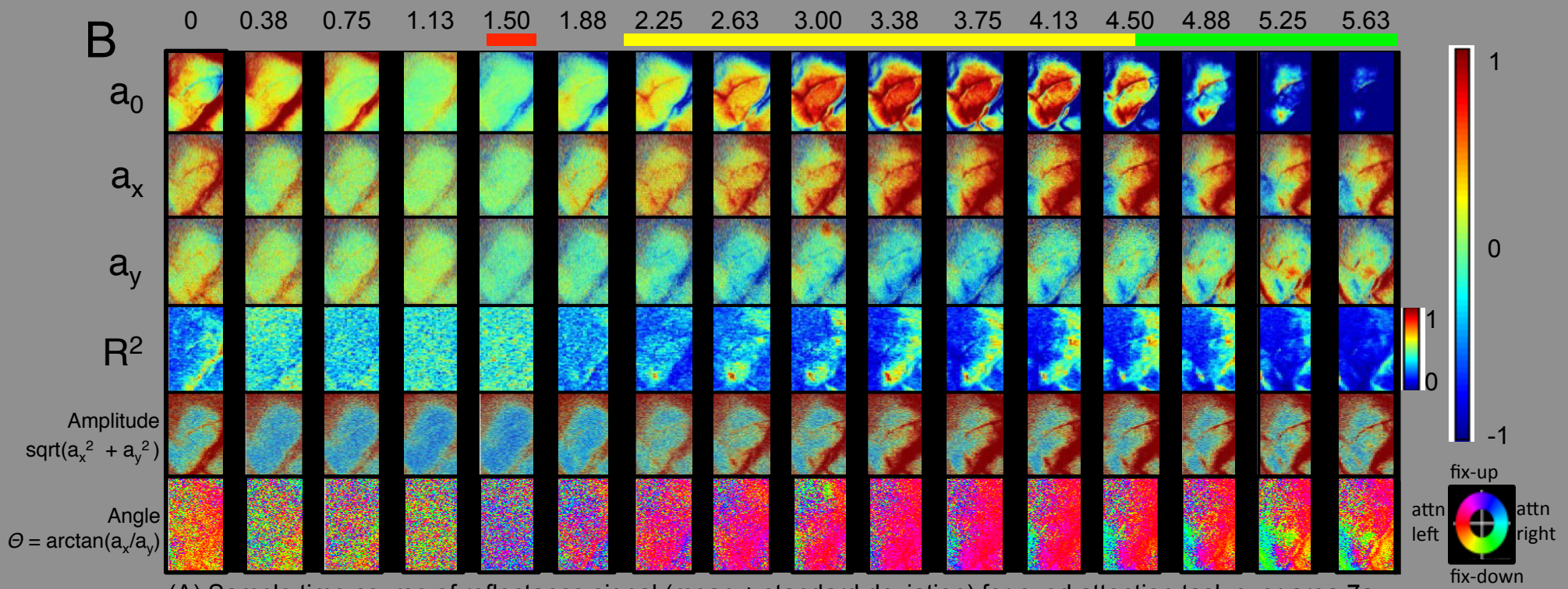

(A) Sample time course of reflectance signal (mean ± standard deviation) for cued attention task over area 7a (left) and area DP (right). (B) Evolution of linear regression parameters during the task. Intercept (a_0), horizontal coefficient (a_x), vertical coefficient (a_y), R^2, vector amplitude, and angle.

Figure 3

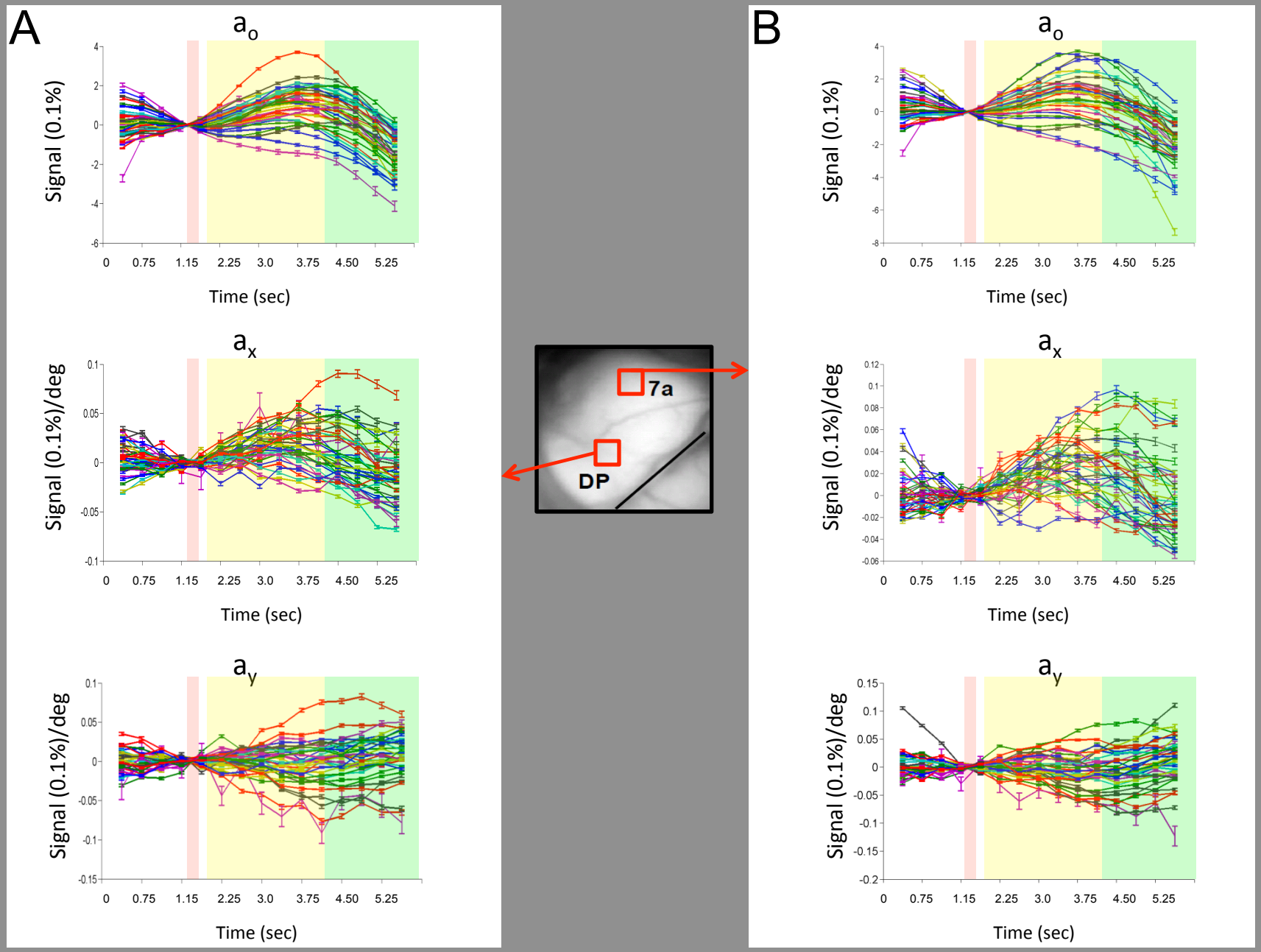

Time course of linear regression parameters (mean ± standard error) for all cued experiments: intercept (a_0), horizontal coefficient (a_x), vertical coefficient (a_y) for area 7a (A) and area DP (B).

Figure 4

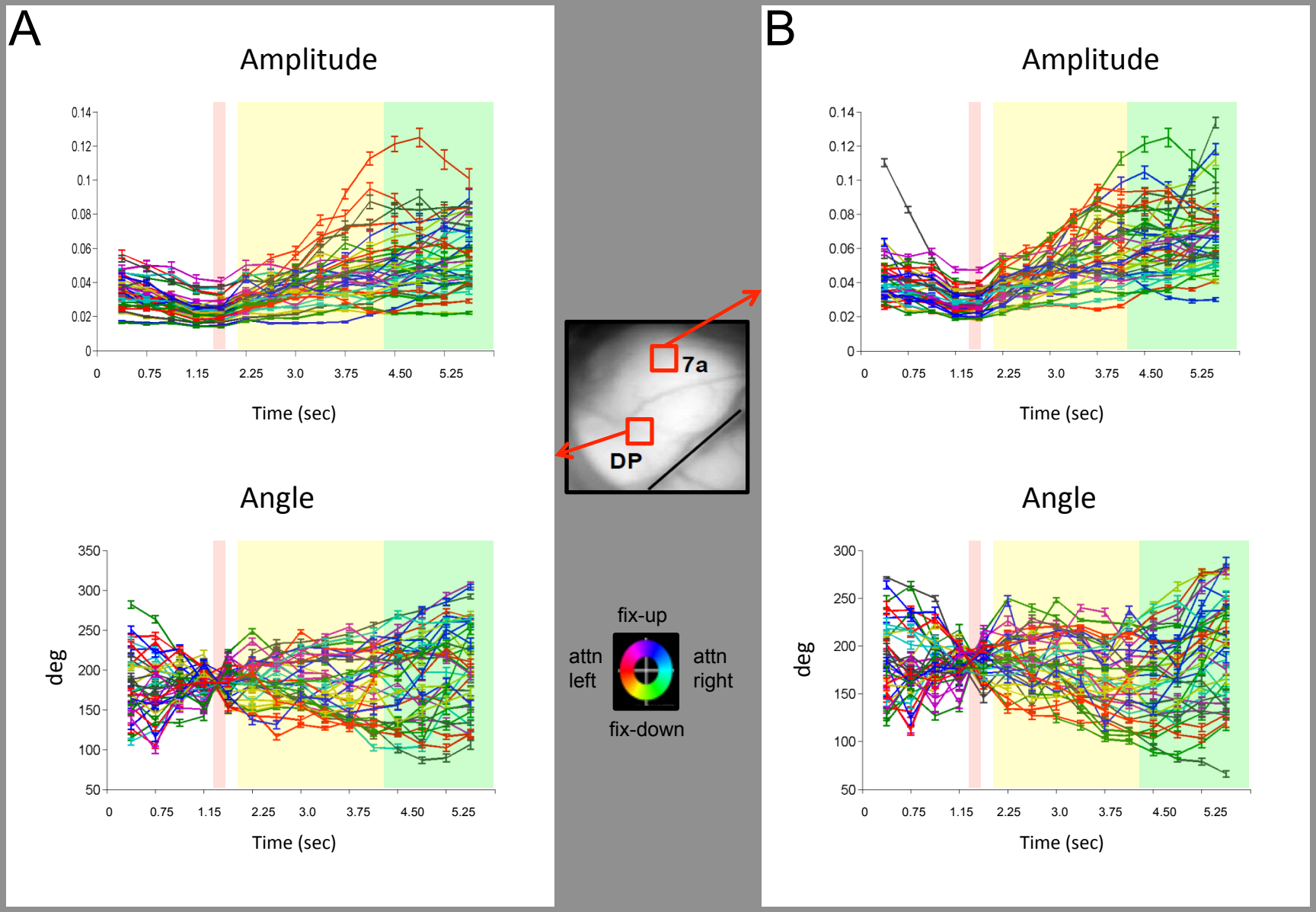

Time course of linear regression parameters (mean ± standard error) for all cued experiments: vector amplitude (top) and angle (bottom) for area 7a (A) and area DP (B).

Figure 5

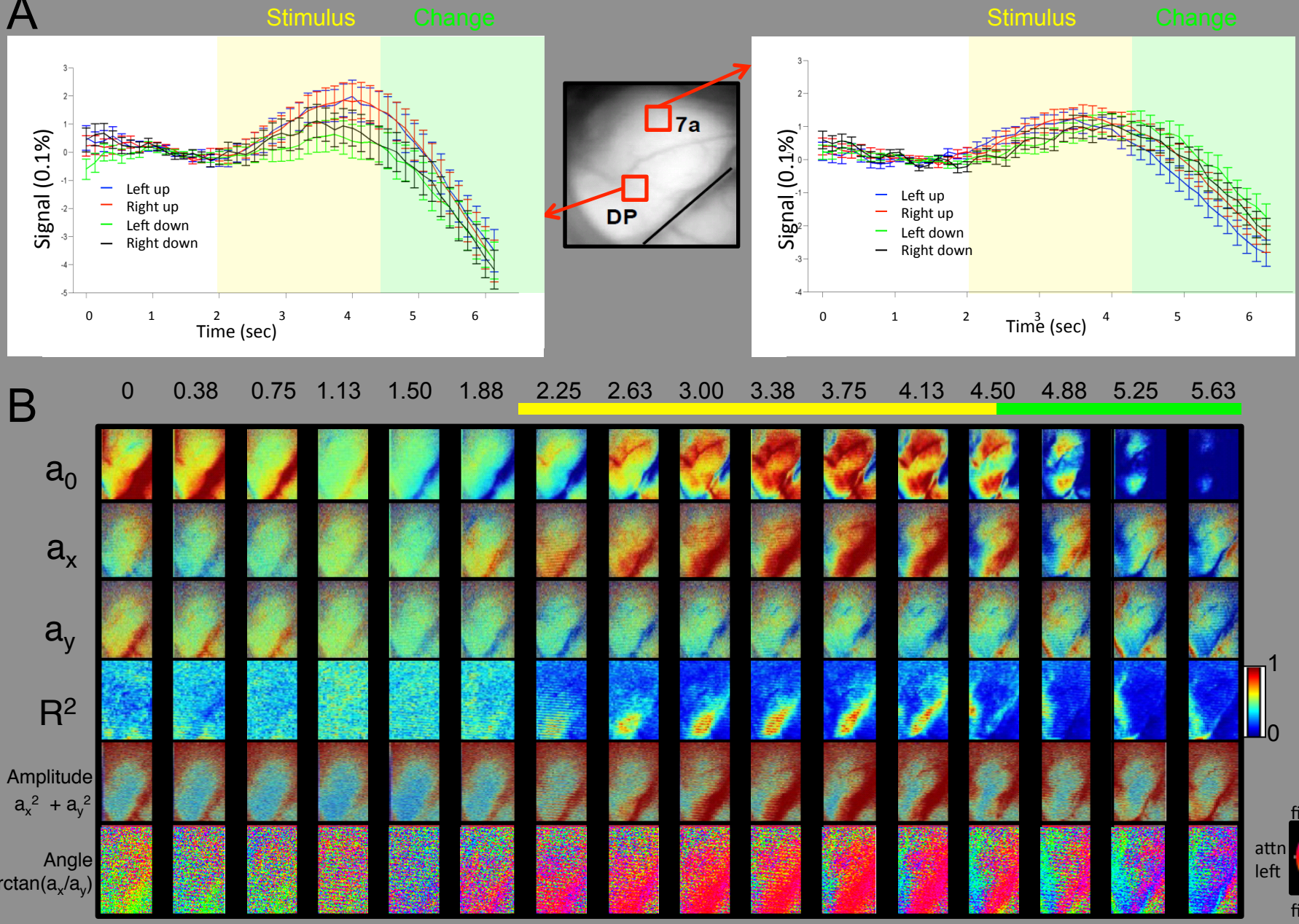

(A) Sample time course of reflectance signal (mean ± standard deviation) for non-cued task over area 7a (left) and area DP (right). (B) Evolution of linear regression parameters during the task. Intercept (a_0), horizontal coefficient (a_x), vertical coefficient (a_y), R^2, vector amplitude, and angle.

Figure 6

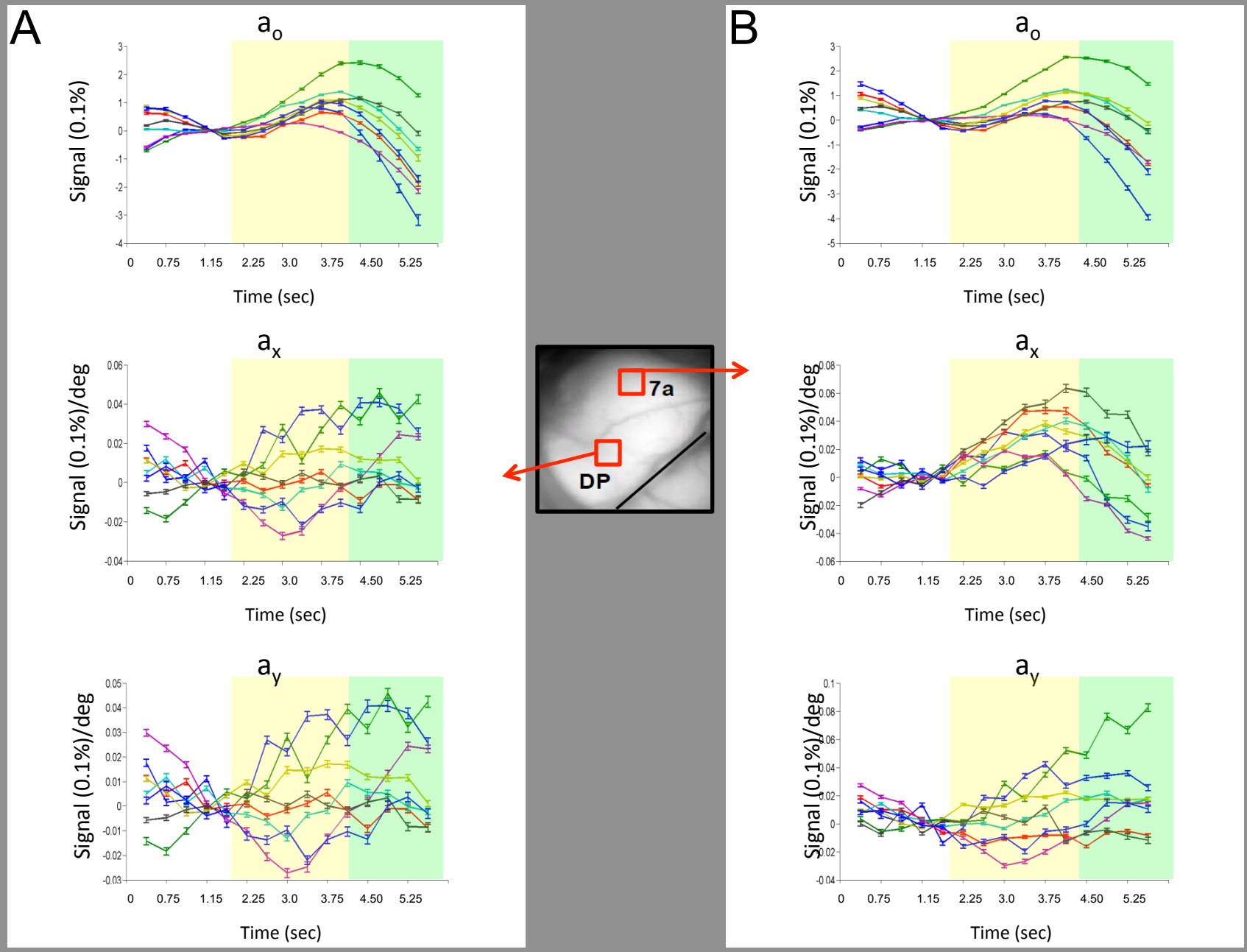

Time course of linear regression parameters (mean ± standard error) for all non-cued experiments: intercept (a_0), horizontal coefficient (a_x), vertical coefficient (a_y) for area 7a (A) and area DP (B).

Figure 7

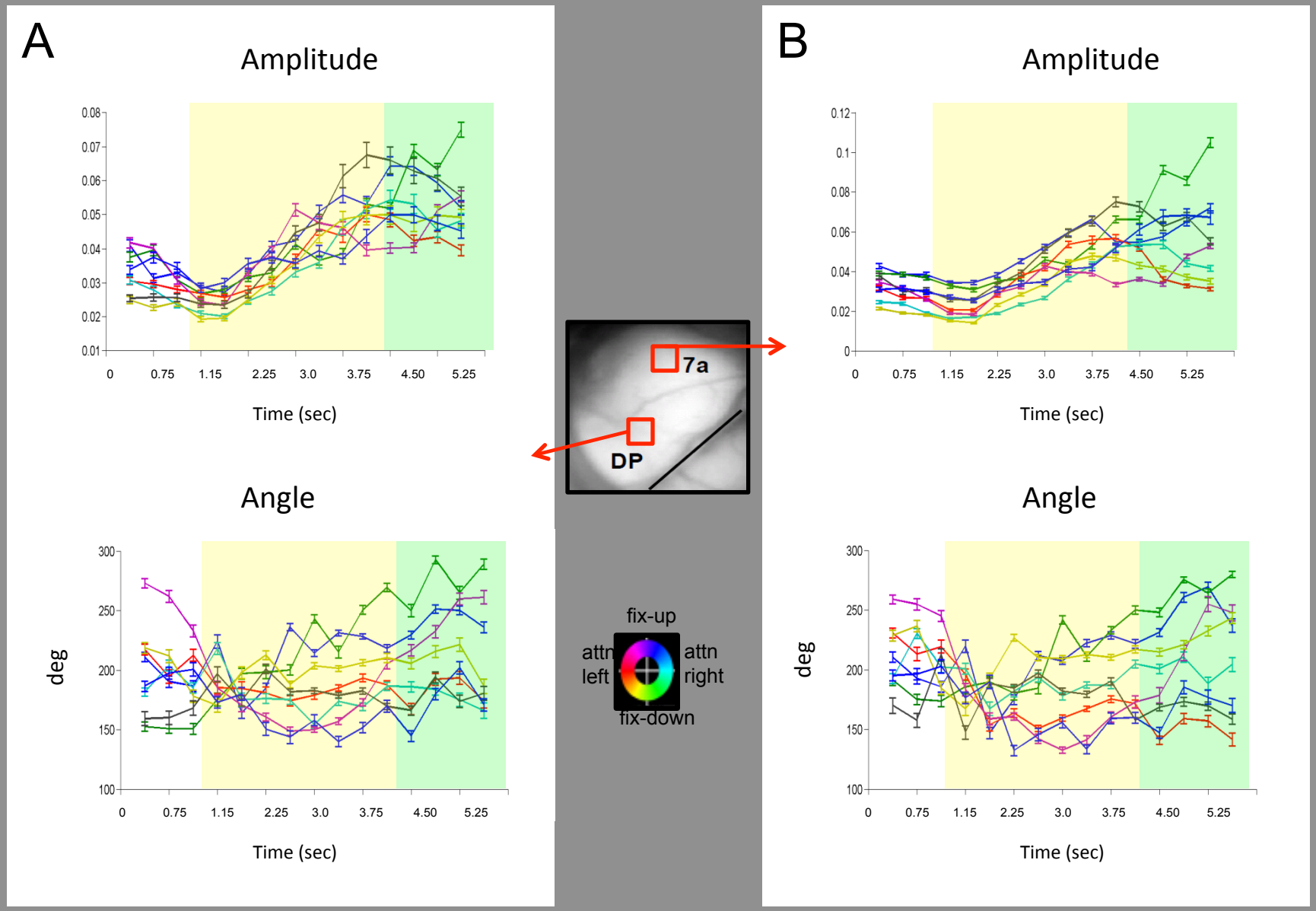

Time course of linear regression parameters (mean ± standard error) for all non-cued experiments: vector amplitude (top) and angle (bottom) for area 7a (A) and area DP (B).

Figure 8

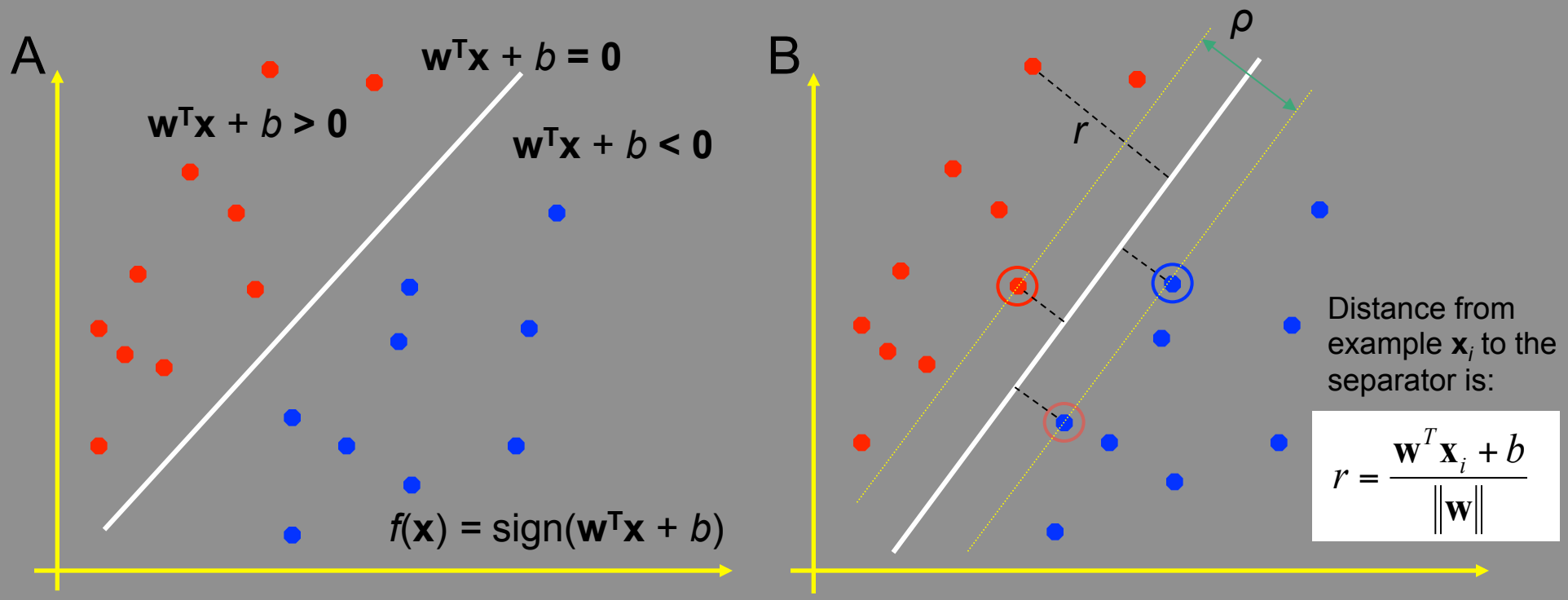

Basic principles of linear support vector machine (LSVM). (A) Binary classification can be viewed as the task of separating classes into feature space. A hyperplane (white diagonal line) separates the two classes. This hyperplane is described by a learning weight vector (**w**) and an offset (b). (B) Classification margin with examples closest to the hyperplane representing ***support vectors***. *Margin ρ* of the separator is the distance between support vectors.

Figure 9

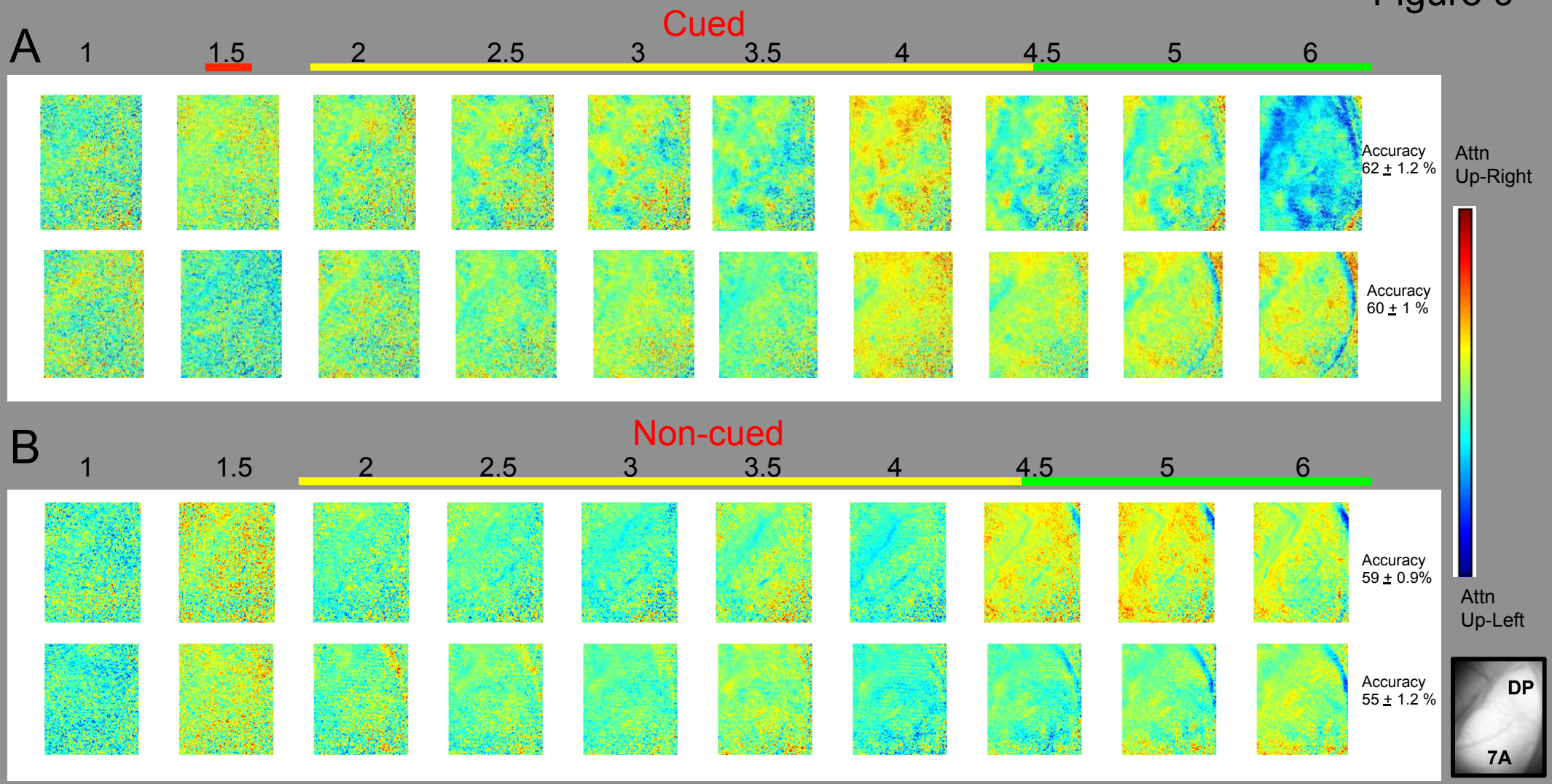

LSVM binary classification for two sample experiments for cued (A) and non-cued (B) tasks plotted for the upper eye position (attention left *vs.* right). For the training, the signal was averaged across all 47 frames to estimate the weight vector (w^T), and then applied to each time segment (4 frames averaged). Overall accuracy does not exceed 62% but certain regions on the map are reliable predictors for attention left (dark blue) or attention right (dark orange).

Figure 10

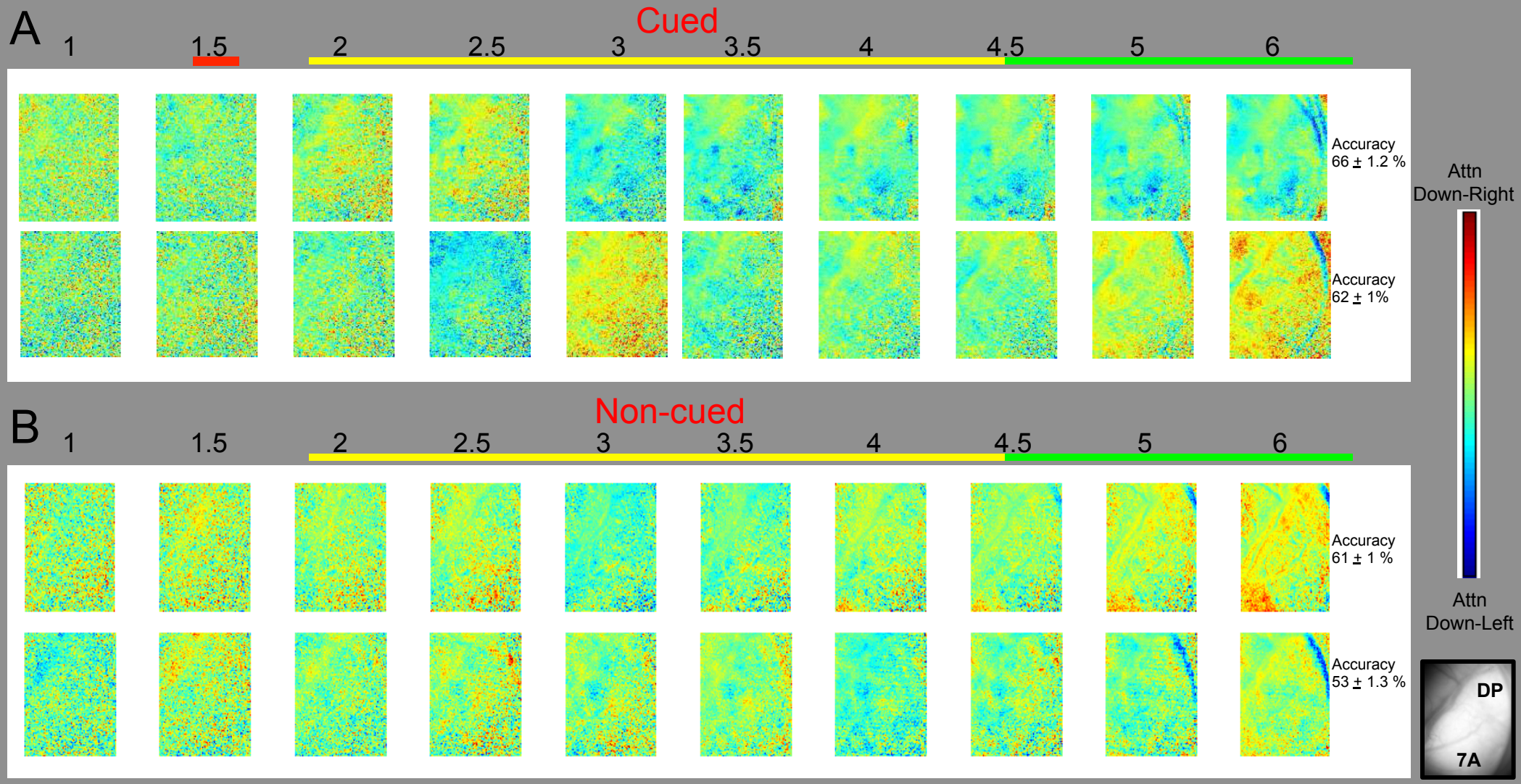

LSVM binary classification for two sample experiments for cued (A) and non-cued (B) tasks for the lower eye position (attention left *vs.* right). For the training, the signal was averaged across all 47 frames to estimate the weight vector (w^T), and then applied to each time segment (4 frames averaged). Overall accuracy does not exceed 66% but certain regions on the map are reliable predictors for attention left (dark blue) or attention right (dark orange).

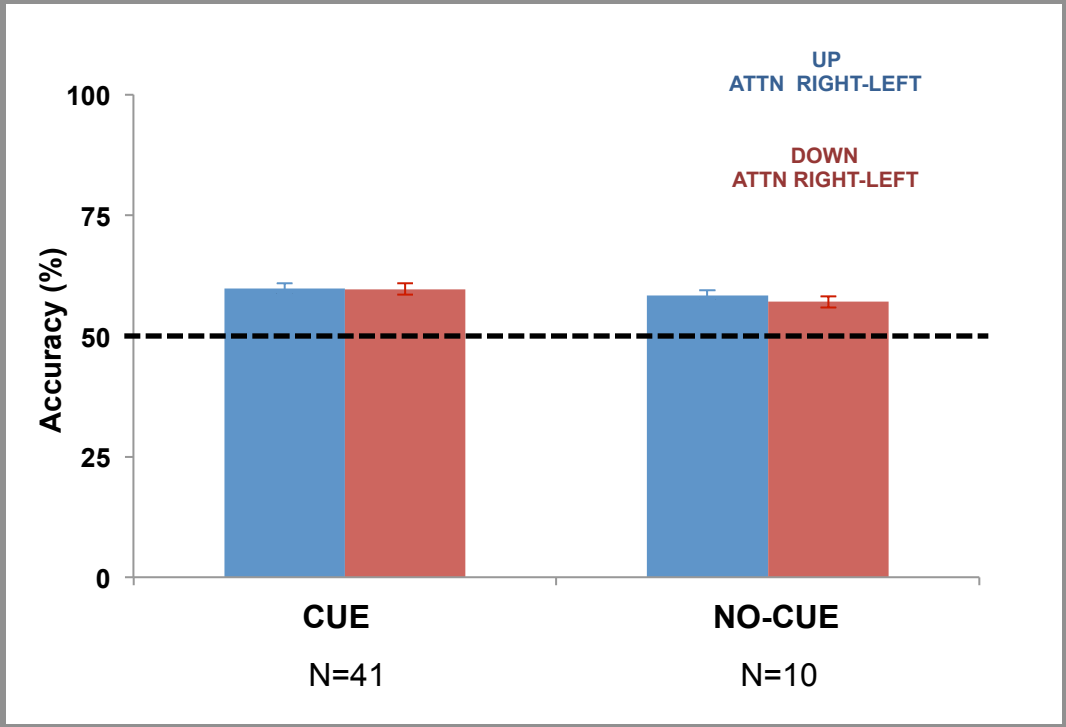

LSVM binary classification accuracy (mean ± standard error) across multiple experiments (cued and non-cued task) separated by eye position (up, blue; down, red). The signal was averaged across all frames to estimate the weight (w^T) and then applied to each time segment (4 frames averaged). Overall accuracy (~60%) is significantly greater than chance (50%).

Figure 12

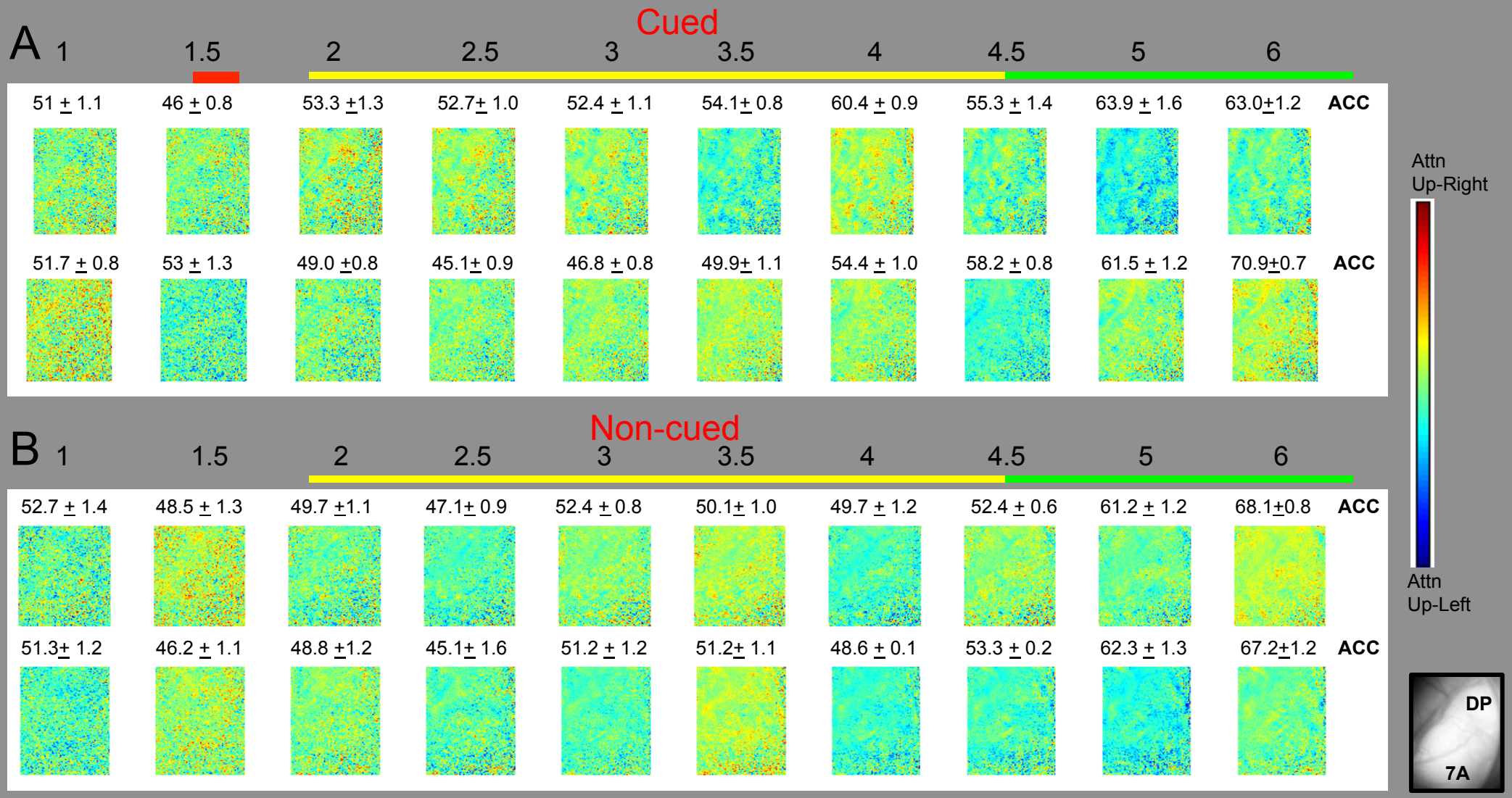

LSVM binary classification for two sample experiments for each cued (A) and non-cued (B) task for the upper eye position (attention left *vs.* right). In these examples, the weight (w^T) was determined for each time segment (4 frames averaged) during training and then applied to each time segment for testing. Over the course of the trial, accuracy improves from chance level (50%) to above 60% for the last segments (~3 s after stimulus onset).

Figure 13

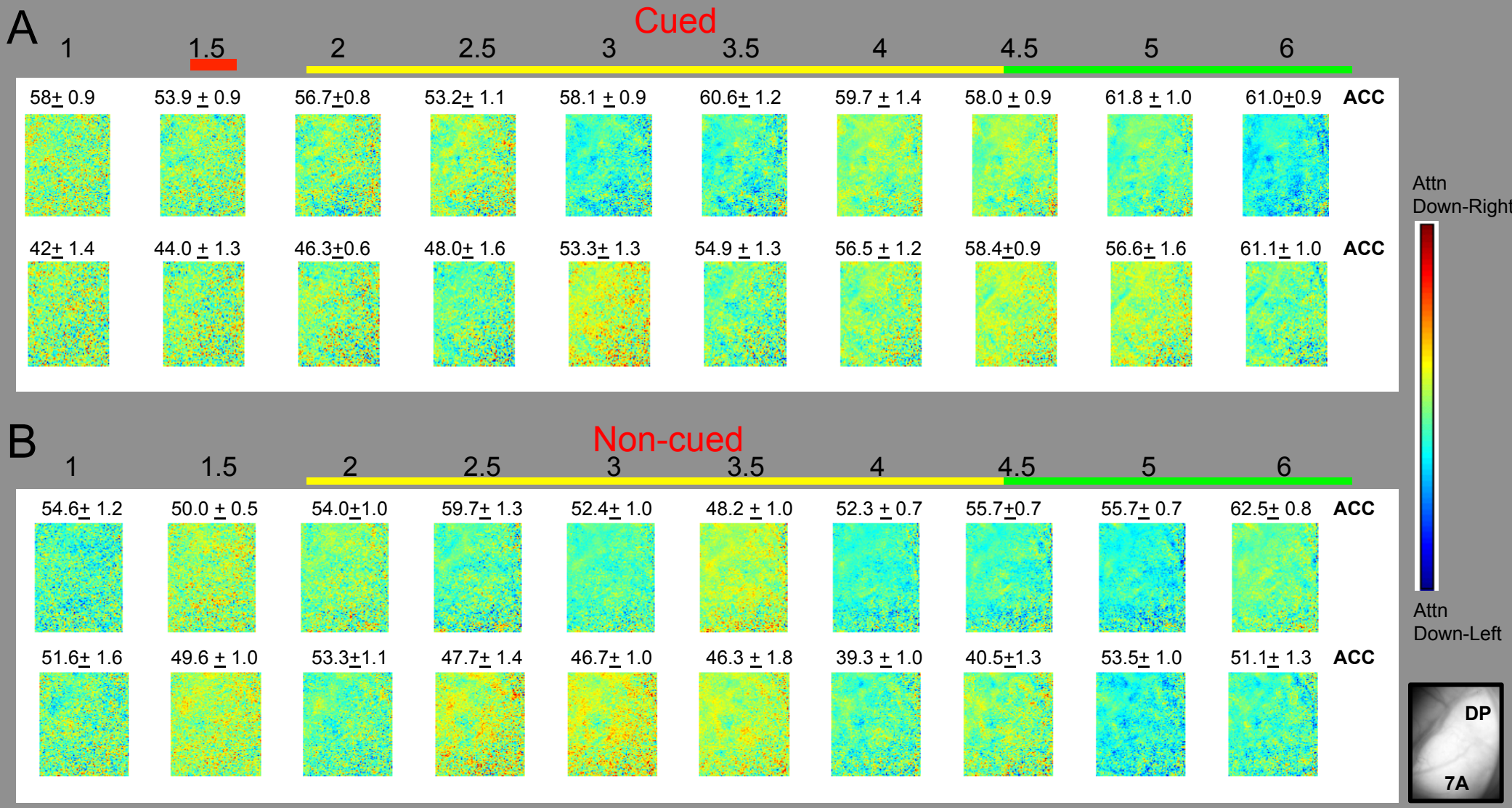

LSVM binary classification for two sample experiments for each cued (A) and non-cued (B) task for the lower eye position (attention left *vs.* right). In these examples, the weight (w^T) was determined for each time segment (4 frames averaged) during training and then applied to each time segment for testing. Over the course of the trial, accuracy improves from chance level (50%) to above 60% for the last segments (~3 s after stimulus onset).

Figure 14

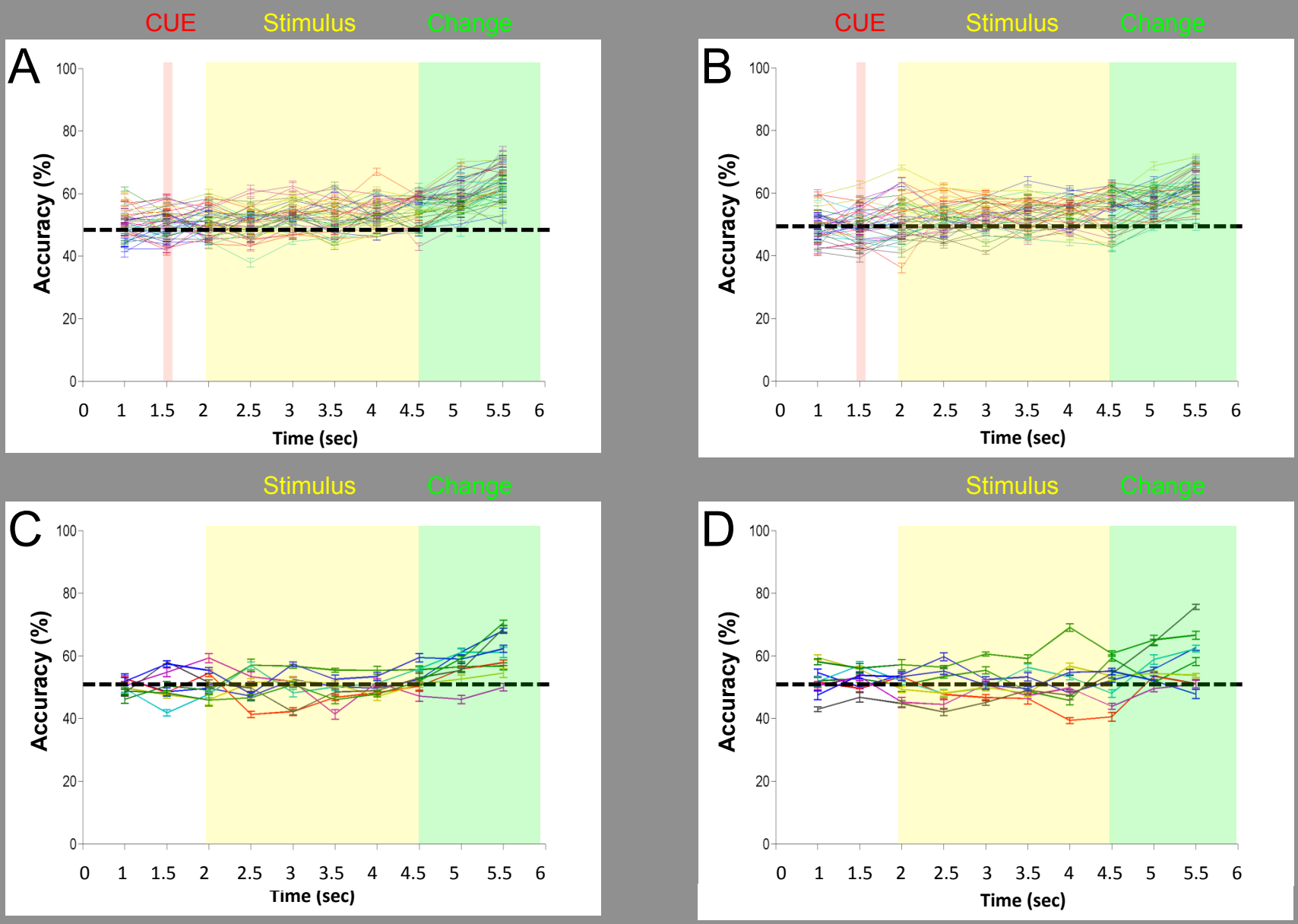

Time course of LSVM binary classification accuracy (mean ± standard error) separated by task condition and eye position. Cued task: (A) upper eye position, (B) lower eye position. Non-cued task: (C) upper eye position, (D) lower eye position. After stimulus onset, accuracy increases gradually from ~50% to ~60% for the last time segments (~2.5s after stimulus onset).

Figure 15

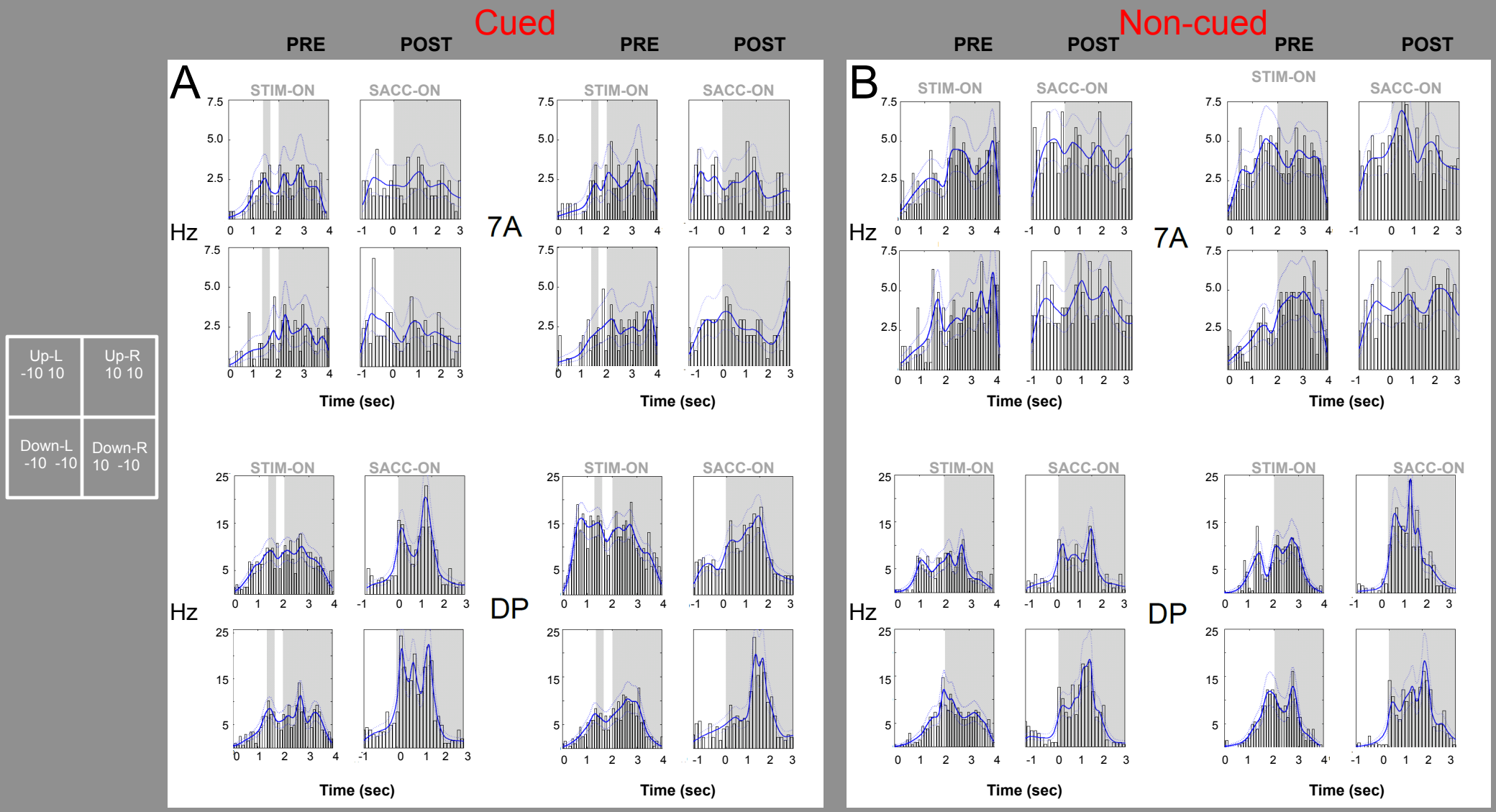

Single unit examples for each area (7a, top panels; DP, bottom panels) during cued (A) and non-cued (B) task. Each pair of panels shows synchronization for stimulus onset (stim-on, PRE) and saccade onset (sacc-on, POST). Panels are arranged according to stimulus conditions indicated to the left.

Figure 16

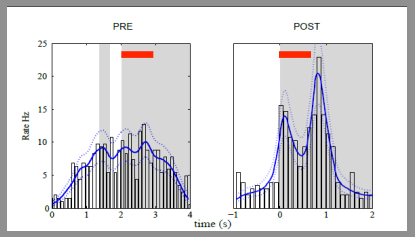

Up-L -10 10	Up-R 10 10
Down-L -10 -10	Down-R 10 -10

Cued

Non-cued

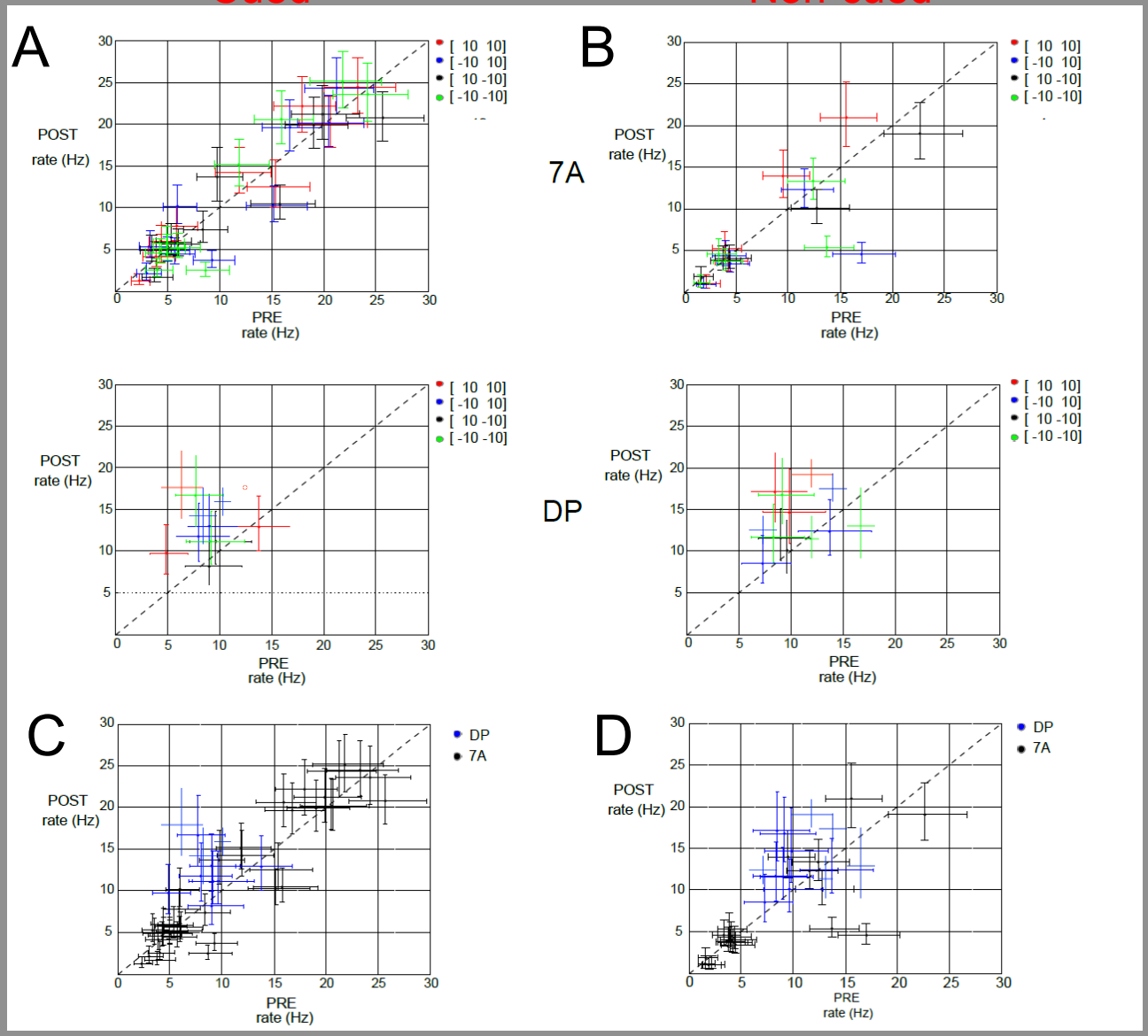

Population single unit analysis from all recorded neurons. Average spike rate from 1 s after stimulus onset (PRE) is compared with average spike rate 1 s after saccade response (POST). (A) Cued task (area 7a, upper panel; area DP, lower panel). (B) Non-cued task (area 7a, upper panel; area DP, lower panel). (C) Inter-areal comparison for cued task. (D) Interareal comparison for non-cued task

Figure 17

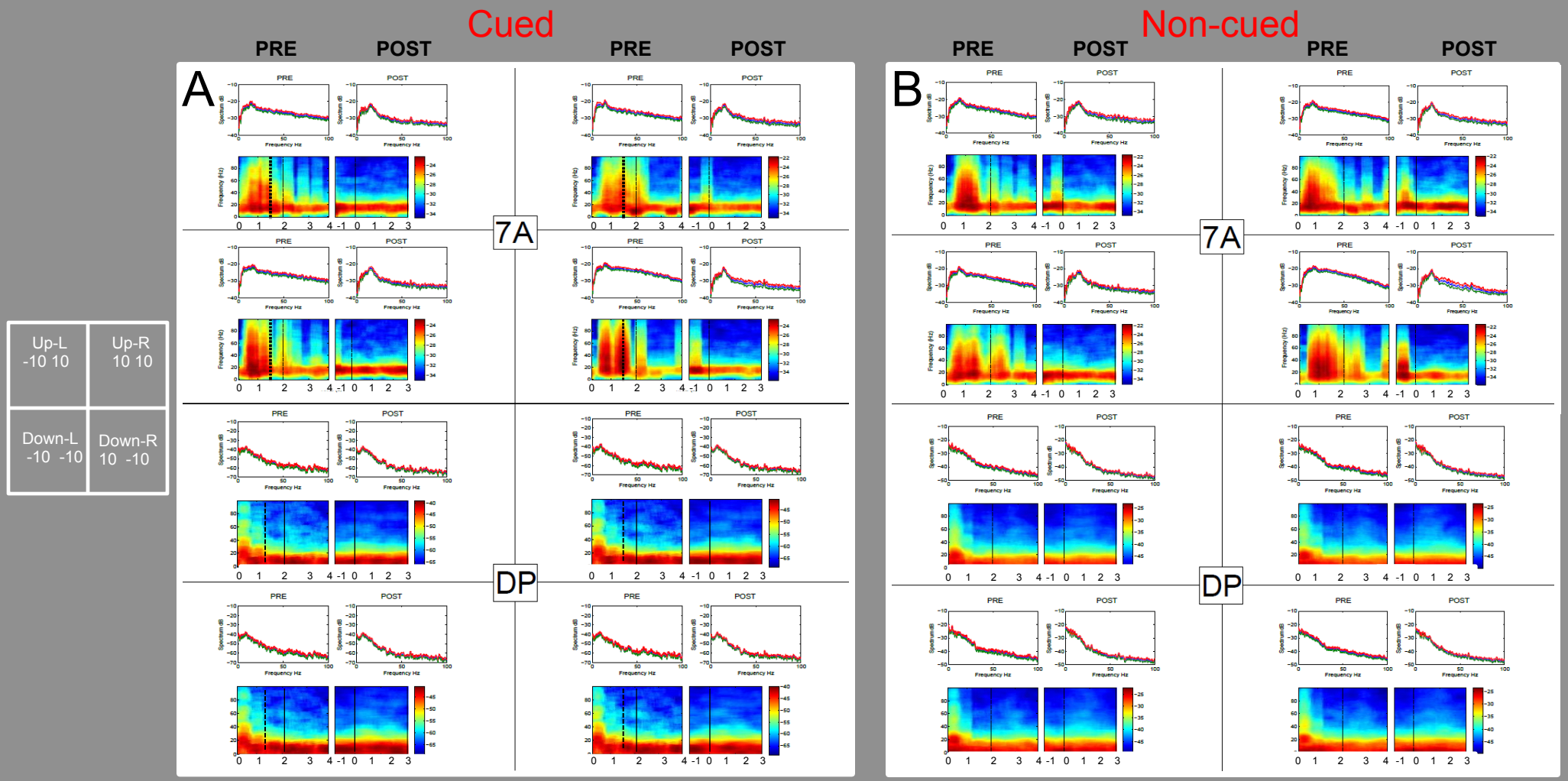

Local field potential analysis for sample sites in each area (7a, top panels; DP, bottom panels) during cued (A) and non-cued (B) task. Each quadrant per area and condition contains two pairs of panels showing the LFP spectrum as a function of frequency (top) and the corresponding color coded spectrograms (bottom, frequency range 10-80 Hz) for the stimulus onset (PRE, left) and saccade onset (POST, right) synchronization. Panels are arranged according to stimulus conditions indicated to the left.

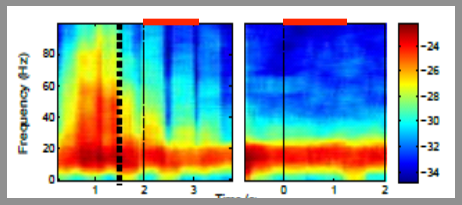

Up-L -10 10	Up-R 10 10
Down-L -10 -10	Down-R 10 -10

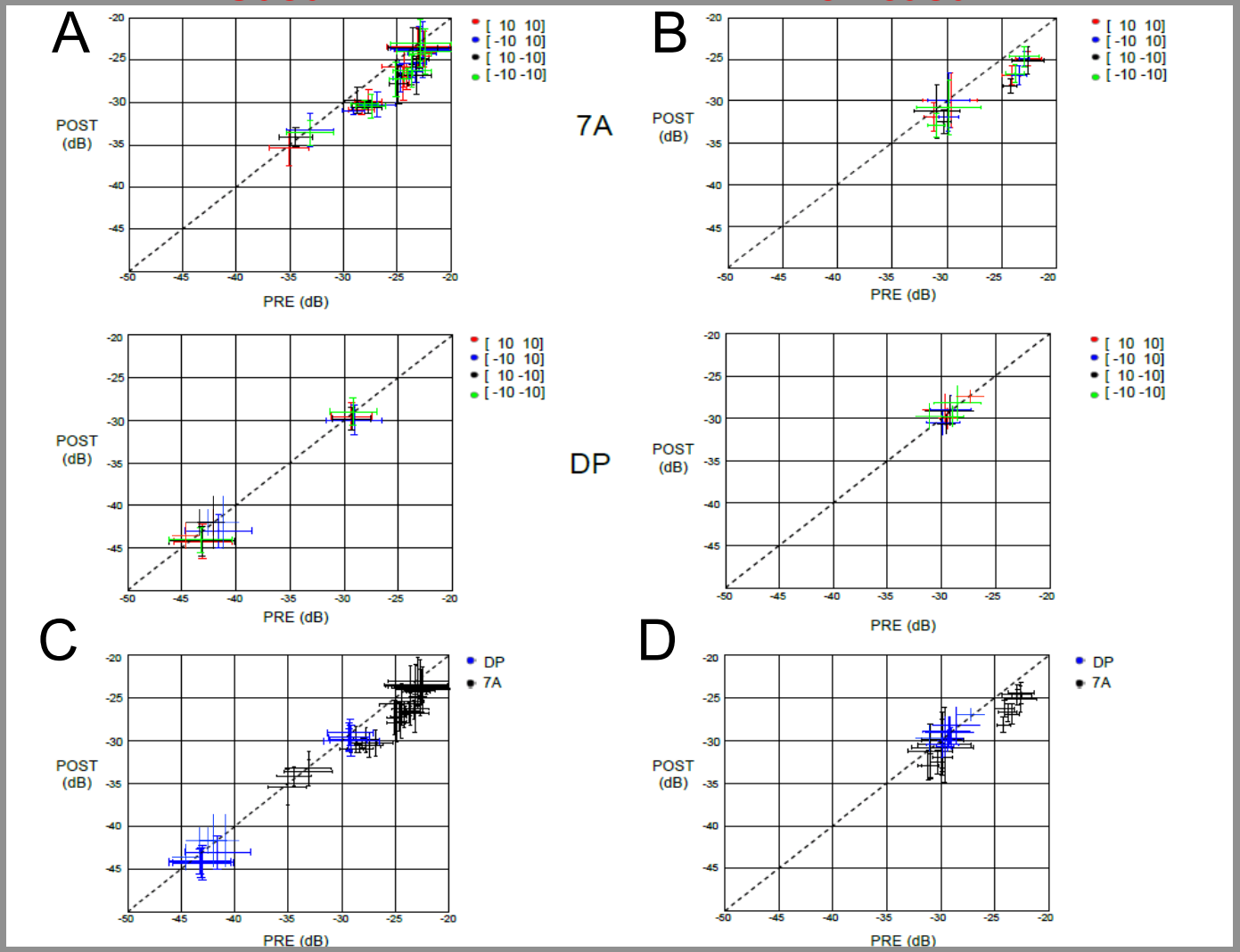

Population local field potential analysis from all recording sites. Average spectrogram 1 s after stimulus onset is compared with average spectrogram 1 s after saccade response, taken from frequency range 5-20Hz. (A) Cued task (area 7a, upper panel; area DP, lower panel). (B) Non-cued task (area 7a, upper panel; area DP, lower panel). (C) Inter-areal comparison cued task. (D) Interareal comparison non-cued task